NINTH EUROPEAN ROTORCRAFT FORUM

Paper No. 57

AEROMECHANICAL ASPECTS IN THE DESIGN OF HINGELESS/BEARINGLESS ROTOR SYSTEMS

V. KLÖPPEL
K. KAMPA
B. ISSELHORST

Messerschmitt-Bölkow-Blohm GmbH
Munich, Germany

September 13–15, 1983
STRESA, ITALY

Associazione Industrie Aerospaziali

Associazione Italiana di Aeronautica ed Astronautica

AEROMECHANICAL ASPECTS IN THE DESIGN OF HINGELESS / BEARINGLESS ROTOR SYSTEMS

V.Klöppel K.Kampa B.Isselhorst

Messerschmitt-Bölkow-Blohm GmbH
Munich, Germany

Abstract

Hingeless/bearingless rotors show pronounced torsion-flap-lag coupling, influencing significantly blade damping, ground and air resonance and general aeromechanical characteristics of the helicopter. These phenomena are discussed with the aid of theoretical models. Special consideration is given to the effect of mathematical modelling on the rotor's dynamic characteristics with regard to rotor inflow and blade damping behaviour.

The theoretical results are verified by whirl tower and flight test data of recent MBB-developments in the field of hingeless and bearingless rotor systems.

Main emphasis is put on aeromechanical investigations, on the influence of particular design parameters on rotor and helicopter stability. Such parameters are for example, the blade droop of the feathering axis, the flexibility of the control system, the rotor flapping and lead-lag stiffness and the pitch-flap coupling.

Notations

$\bar{a}_\beta$	equivalent flapping hinge offset
C_β	equivalent flapping hinge restraint
C_ζ	equivalent lagging hinge restraint
$C_{\theta CT}$	control stiffness
$D_{\zeta STRUC}$	inherent lead-lag damping
$D_{\Omega-\omega_\zeta}$	fixed system damping of lead-lag regressing mode
$D_{\dot{\zeta}}$	lead-lag damping, rotating system
m_{TO}	gross weight
M_β	flapwise bending moment
M_ζ	inplane bending moment
M_θ	pitching moment
R	rotor radius
V_x	horizontal flight velocity
β, β^*	flapping angle
β_{BB}	blade-to-beam predroop angle
ζ, ζ^*	lead-lag angle
δ_1	pitch-lag coupling
δ_3	pitch-flap coupling
$\theta_{C\dot{T}}$	elastic pitch angle
$\Omega, \bar{\Omega}$	rotor speed
ω_ζ	natural lead-lag frequency

1. Introduction

In the development of rotor systems two different ways exist to replace the common flapping and lead-lag hinges as well as the pitch bearing:

- the introduction of elastomeric hinges and bearings and
- the use of elastic properties of the blade root to provide the blade motions.

After the design of the BO 105 main rotor system, which has been a first step in the latter direction, the bearingless main rotor is a consequent progression (see Figure 1.1).

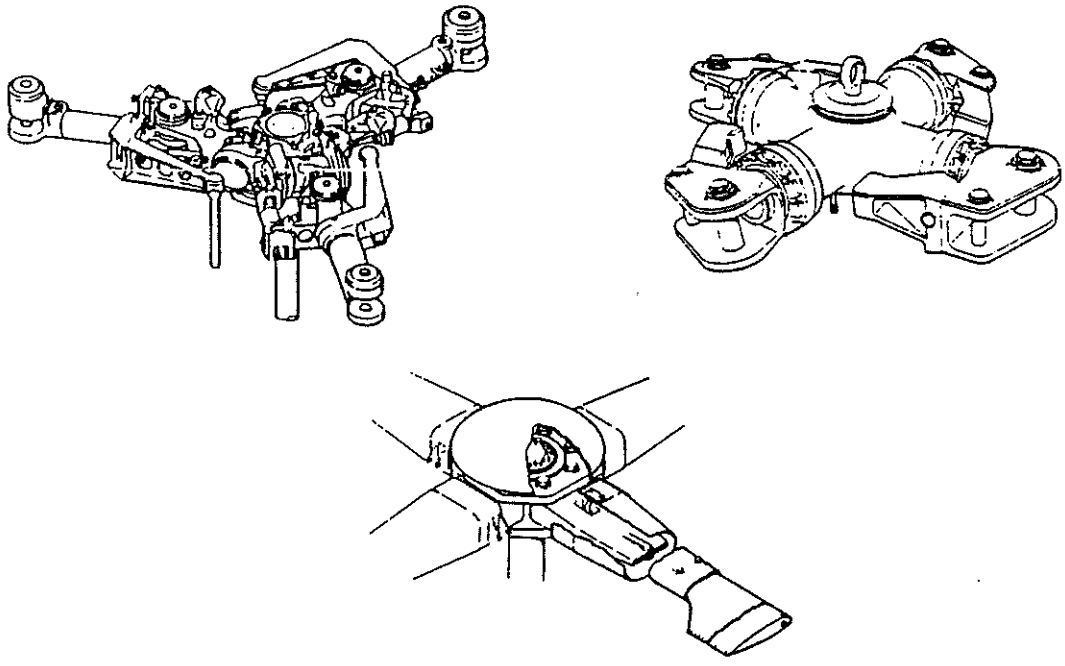

Figure 1.1 Development of rotor systems

The development of a bearingless tail rotor has made similar progress at MBB. Experimental versions of both rotor systems are presented in Figure 1.2. The primary goals of these developments are a reduction in complexity, a longer life span, and lower weight.

The design of new rotor systems gives rise to a number of aeromechanical phenomena and problems, some of which are the subject of this paper.

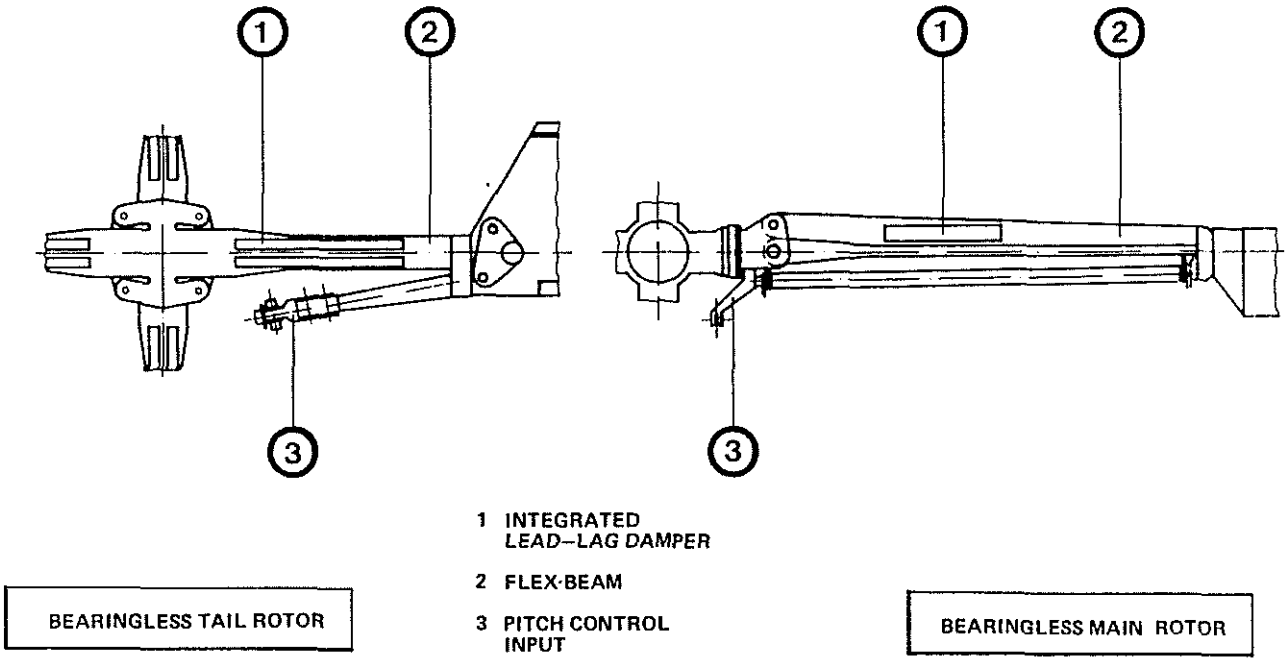

Figure 1.2 Experimental versions of MBB-bearingless main and tail rotor

2. Description of the Bearingless Rotor System

In the past, a small number of bearingless rotor systems have been developed and tested (references 8,9,10,11,12). All these prototype designs have shown a multitude of configurations especially in the flex-beam assembly. Two experimental versions of several bearingless main rotor systems, presently in development at MBB, are shown schematically in Figure 1.2. Following MBB's general rotor concept the rotors are soft-inplane systems (main rotor: $\bar{\omega}_\zeta = 0{,}70$; tail rotor: $\bar{\omega}_\zeta = 0{,}77$). One of the two most important components, typical for this rotor system, is the flex-beam, because of the many tasks it has to accomplish, such as:

- feathering for blade pitch changes
- transmitting of the blade forces and moments to the hub
- sustaining the centrifugal forces
- fulfilling the requirements of frequency design for flap and lead-lag motion
- favourable positioning of the axis of gravity centers, shear centers and tension centers to avoid unexpected bending-twist couplings.

The second important and characteristic component of the bearingless rotor system is the pitch control configuration, which may be a cuff, one or two torque tubes or a cantilever pitch arm as for the bearingless tail rotor configuration of Figure 1.2.

Main tasks of this part are:

- accomplishment of blade pitch via an attachment point located beyond the flex-beam
- performance of flap and lead-lag motions simultaneously to the elastic blade root bending.

It is part of the design philosophy at MBB to use aeroelastic coupling effects, produced at the flexible roots of the hingeless fiberglass blades. It is known from experience that the aeroelastic bending coupling behaviour of hingeless rotor blades is mainly influenced by the position of the blade relative to the control axis. This is particularly cumbersome to determine in the case of the various bearingless rotor concepts (references 2,4), because one has to take into consideration out-of-plane bending of the blade root (flex-beam) as well as bending of the control device. The present paper describes and uses an analysis applying an equivalent system technique, where this position is determined with the help of the blade-to-beam angle β_{BB}. However, the built-in value of this parameter may change elastically depending on flight condition. Therefore, the actual size of the effective blade-to-beam angle β_{BB} has to be previously estimated with the help of a specialized beam theory or finite element method.

3. Mathematical Modelling

As shown in Figure 3.1 the kinematics of bearingless rotors are mathematically simulated by equivalent hinges, springs, and dampers, which represent the first modes in flap, lead-lag, and torsion. Higher modes than the first are neglected, because they are not needed for low-frequency aeromechanical stability analysis.

In the same manner, single modes of fuselage, tailboom or test stand rolling, pitching and yawing at ground resonance conditions are also idealized (see Figure 3.2). For air resonance conditions, springs and dampers below the fuselage are set zero.

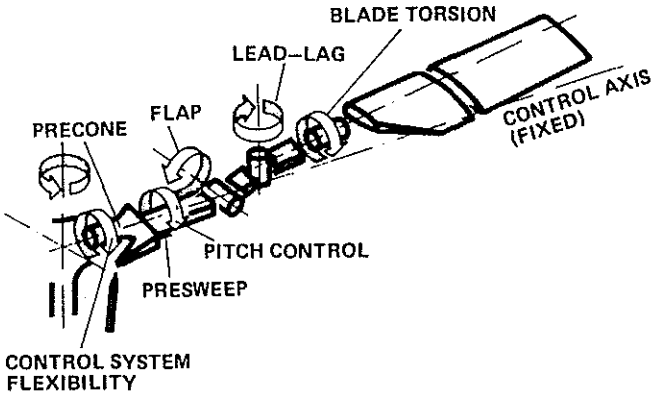

ROTOR SYSTEM BO 105

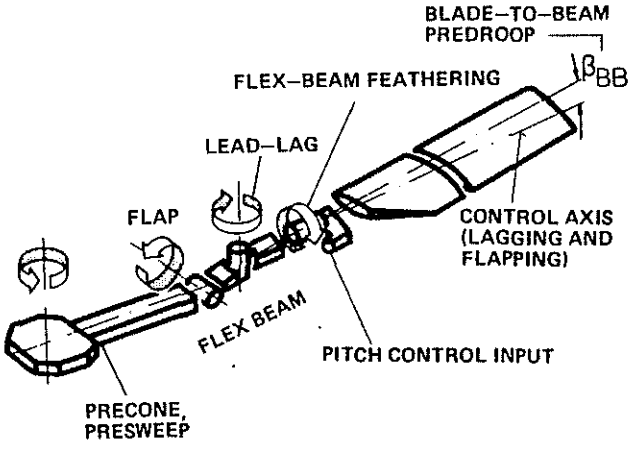

BEARINGLESS ROTOR SYSTEM

Figure 3.1 Mathematical modelling of hingeless and bearingless rotor system

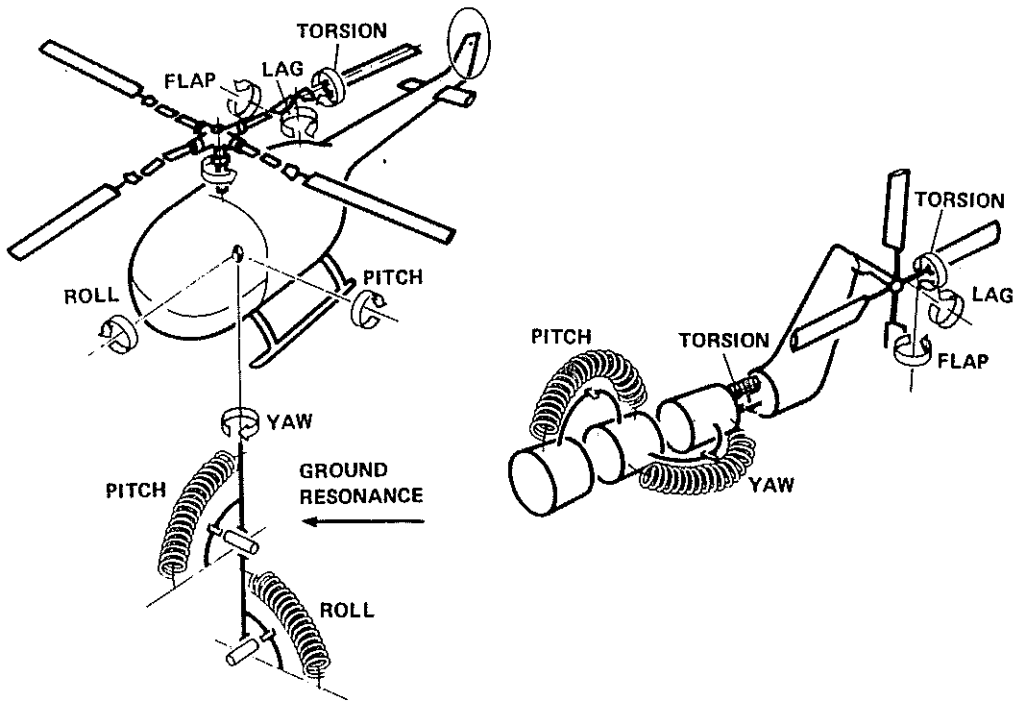

Figure 3.2 Mathematical ground and air resonance models

The aerodynamic calculation model is based on current blade element theory. The rotor inflow is calculated in most cases as constant above the rotor disc, with a trapezoidal inflow distribution in forward flight. In the regime of vortex-ring state and hovering, the induced velocity is computed from an empirical data list. A more complex inflow model, based on a local momentum theory, is additionally used, considering azimuthal and radial sections of the rotor disc. This inflow model has, for example, been applied to reproduce the whirl tower test results of the bearingless main rotor.

The structural damping values stem from measurement results and are considered constant. In reality, a nonlinear dependence of inherent lead-lag damping of lead-lag amplitude, for example, seems to be reasonable, depending on the particular rotor system (see chapter 6.3).

The calculation of the system behaviour begins by establishing trimmed conditions for the degrees of freedom of the blade and the helicopter as a whole. Starting from this distinct equilibrium condition, belonging to an optional flight situation, which has been achieved by integration of a nonlinear differential equation system, a perturbation analysis is accomplished yielding derivatives needed for the calculation of first order stability equations. This linear equation system is solved as a conventional eigenvalue problem.

Instead of stability analysis, the trim calculation may also be followed by a time history computation.

4. Dynamic Coupling Effects

In order to explore the basic physics of dynamic coupling effects of the rotor blade, besides the complex aeromechanical mathematical model shortly presented in chapter 2 and 3, a simplified physical approach will be used.

4.1 Elastic Pitch-Lag Coupling (δ_1)

One important property of bearingless rotors is the almost fixed position of the blade relative to the control axis in an actual trimmed flight condition. This is valid especially for the configuration with low equivalent flapping hinge offset and zero blade-to-beam predroop angle. In this case, the flapping angle of the blade is nearly identical to that of the control assembly (cuff or torsion tube), and therefore no deflection of the blade exists relative to the simultaneous flapping and lagging control axis. Under these circumstances, it is expected that no elastic δ_3 or δ_1 coupling will occur.

Nevertheless, it is possible to create a virtual or elastic pitch-lag coupling with the help of parameters discussed later on.

For the explanation of the δ_1-coupling it is helpful to use a simplified physical modelling similar to reference 1. Equating to zero the sum of twisting moments per unit length about the control axis is

$$M_\theta = -M_\beta \cdot \zeta^* + M_\zeta \cdot \beta^* \ldots\ldots\ldots, \qquad (1)$$

where ζ^* and β^* are the flap and lead-lag angles with respect to the control axis. Looking at equation 1, it is obvious that the torsional moment due to blade bending is only produced if flap or lag moments exist, and the angles β^* or ζ^* are not zero. Within this physical treatment, the first derivation of equation 1 after the elastic lead-lag angle gives

$$\frac{\partial\theta_{CT}}{\partial\zeta} = f\ (\ldots,\ \beta^* \frac{C_\zeta}{C_{\theta CT}},\ldots) \qquad (2)$$

which yields the main contribution to the pitch-lag coupling angle $\delta_1 = \partial\theta_{CT}/\partial\zeta$.

Equation 2 denotes the parameters which mainly act on the δ_1-coupling: first, the effective blade-to-beam precone angle β_{BB} which is identical with β^* for all bearingless main rotor configurations discussed in this paper and second, the ratio of lead-lag and control stiffness $C_\zeta / C_{\theta CT}$.

4.1.1 Blade-to-Beam Predroop Angle

For rotor trim situations including only the first blade harmonics the influence of the δ_1-coupling can be seen distinctly. Figure 4.1 shows the correlation of the elastic feathering of the control system (cuff or torsion tube) and the elastic lead-lag angle ζ. The inclination of this θ- ζ-loop, visualizing the magnitude of the pitch-lag coupling, is strongly influenced by the effective blade-to-beam predroop angle. A positive δ_1-coupling points out rearward lagging and elastic nose-up pitching of the blade. This kind of δ_1-coupling has a stabilizing influence on lead-lag modes (see chap.6). The direct relation between effective blade-to-beam predroop angle and δ_1-coupling is plotted in the small subpicture of Figure 4.1.

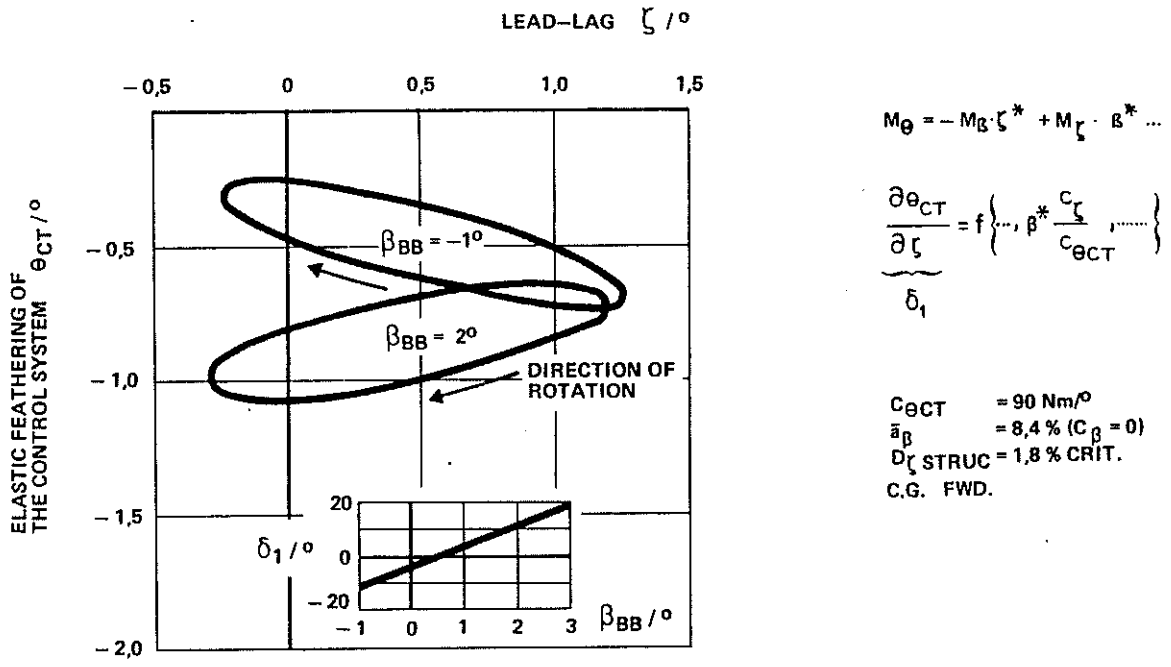

Figure 4.1. Elastic pitch-lag coupling of bearingless main rotor in hover dependent on the blade-to-beam angle

For the selected rotor configuration it can be seen that, at about 0,5 degrees of blade-to-beam predroop angle the δ_1-coupling will vanish - if so desired. It should be noted that the δ_1-coupling must be carefully optimized because it influences not only the blade motion but also the handling qualities of the whole helicopter, such as cyclic control moment or pitch roll coupling.

4.1.2 Control Stiffness

The spring characteristics of torque tube or cuff, swash plate, and pitch control assembly are included in the stiffness parameter $C_{\theta CT}$. By variation of this parameter, similar effects as with the help of the blade-to-beam angle, can be obtained (see Figure 4.2). However, control stiffness variation is less effective within the bounds of constructive possibilities (see sub-picture of Figure 4.2). Beyond that, the magnitude and sense of the produced influence depends on the basic coupling behaviour of the rotor system.

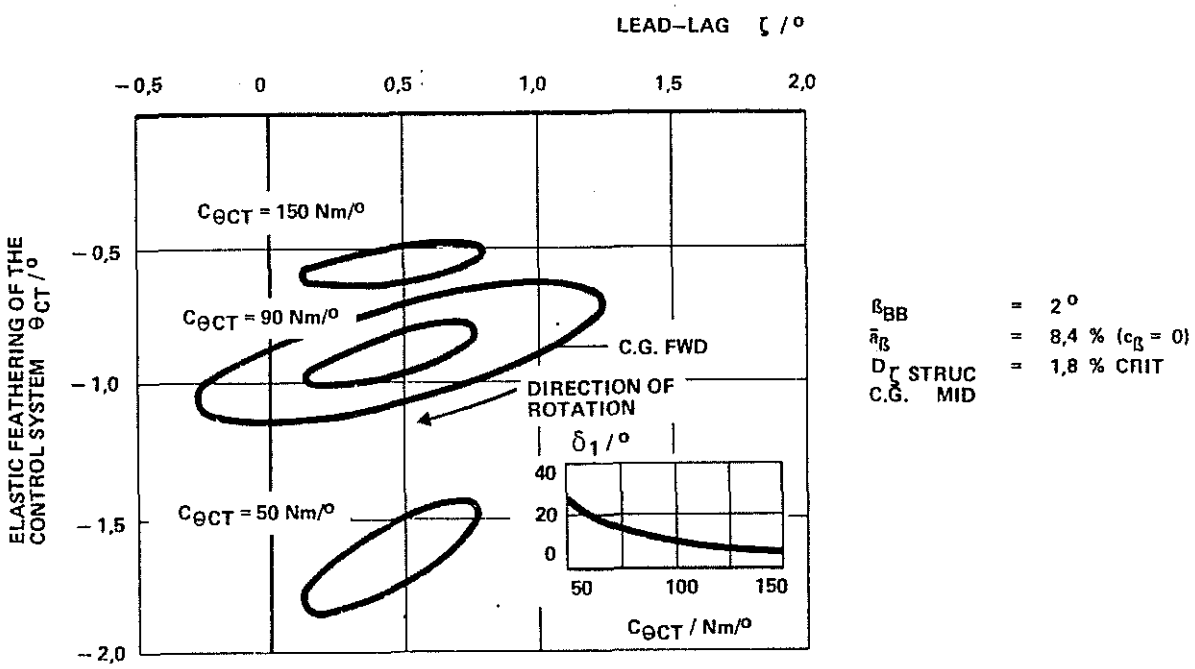

Figure 4.2 Pitch-lag coupling of bearingless main rotor in hover depending on the control stiffness of the cuff assembly

4.2 Pitch-Flap Coupling (δ_3)

As already mentioned, the elastic motion of the blade relative to the simultaneous lagging and flapping control axis is minimized for the bearingless main rotor configuration of Figure 1.2.

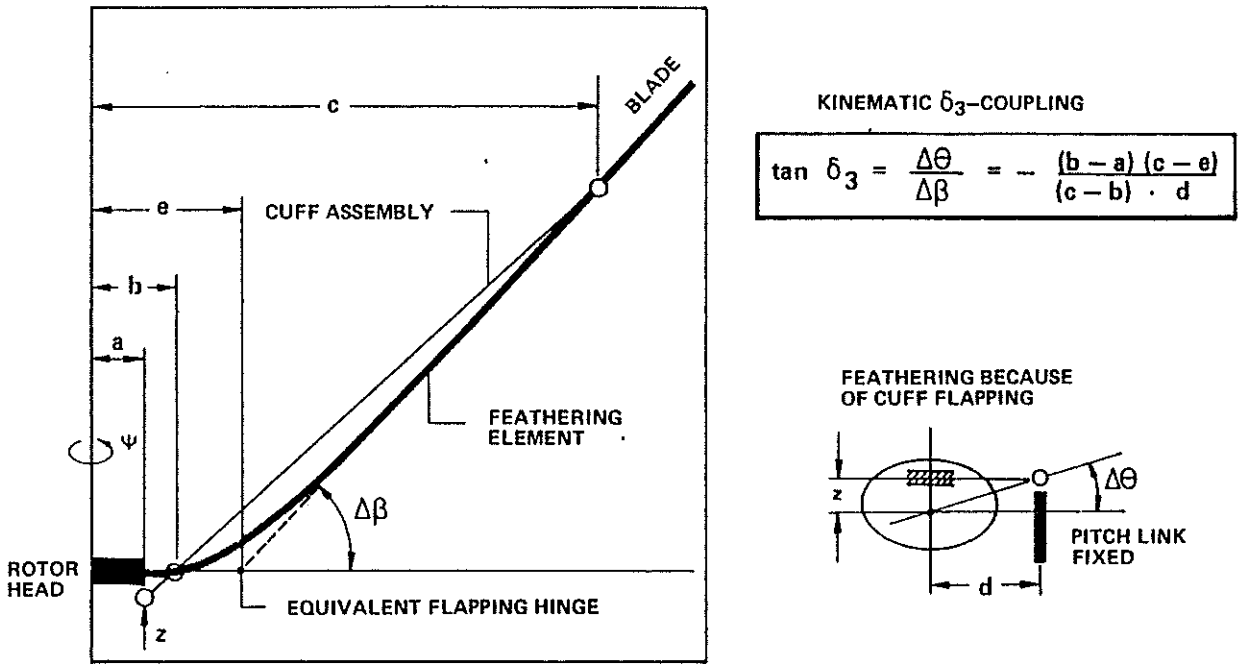

Figure 4.3 Configuration of kinematic δ_3-coupling on bearingless rotor system

With the help of equation 1 one can verify that with $\zeta^* = 0$ no torsional moment is created by flapping.

Nevertheless, it is possible to create a kinematic δ_3-coupling for the bearingless rotor system (see Figure 4.3), which is otherwise difficult to realize on common hingeless rotor systems (reference 3).

Variation of this coupling parameter is known to have significant but contradictory effects on flight dynamic characteristics and rotor blade motion stability (see chapter 6.1 and reference 13).

Besides, a pitch-flap coupling is possible by chordwise offsets of center of gravity or aerodynamic center. Effects of these offsets on blade dynamics arise, in the case of c.g.-displacement, mainly from centrifugal forces if the blade flaps out of the rotor plane. In the case of a.c.-displacement an aerodynamic pitching moment of the blade is directly generated.

As both types of offsets work on bearingless main rotors in the same manner as on common hingeless rotors, these influences are not discussed in more detail.

It should be noted in conclusion, that c.g.-a.c.-offsets do not influence the pitch-lag coupling in an appreciable manner.

5. Ground Resonance and Lead-Lag Damping Situation of Existing Rotor Projects

5.1 Lead-Lag Damping during Whirl Tower Tests

Tests were conducted, on a whirl tower, with an experimental version of the bearingless MBB main rotor, with

- built-in blade-to-beam angle $\beta_{BB} = 2°$
- control stiffness $C_{\theta CT} = 94$ Nm/°
- pitch flap coupling $\delta_3 = 0$

Under centrifugal force, the blade-to-beam angle decreases noticeably, depending on thrust conditions. For theoretical evaluations, a calculated mean value of $\beta_{BB} = 0{,}8°$ has been introduced.

To increase structural damping a constrained layer damper (viscoelastic damping material) has been integrated in the rotor system. Component measurements showed a damping contribution of about 0,5% crit.

In spite of the above mentioned steps, the lead-lag damping level of the bearingless main rotor is about 1% lower than the hingeless rotor level (see Figure 5.1).

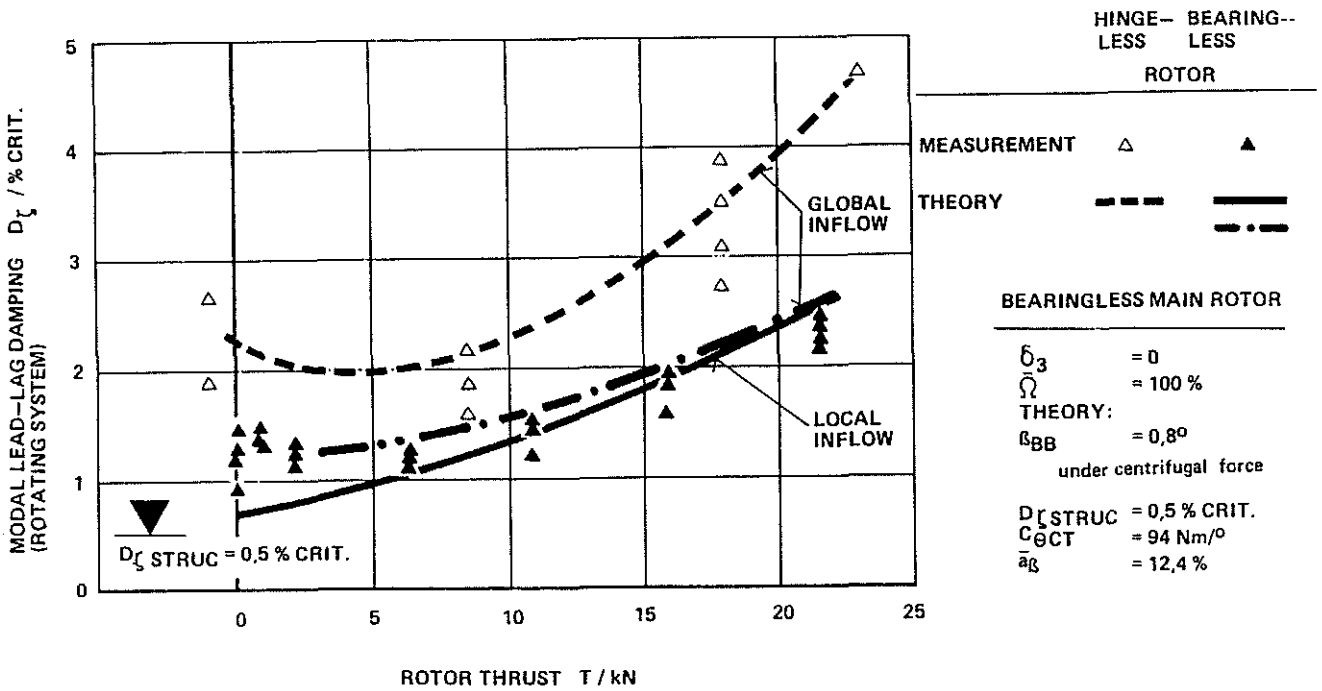

Figure 5.1 Lead-lag damping of bearingless main rotor - experimental version - and BO105 hingeless rotor (whirl tower test)

This might be caused by a different inherent damping (different interlaminar shear stresses) in the region of the blade-to-hub attachment fittings.

The theoretical results, shown in Figure 5.1, are evaluated both with global and local inflow models. The global inflow model does not account for induced flow perturbations, whereas the local inflow iteration, based on the thrust of individual rotor disc elements, provides a more realistic non-uniform downwash flowfield. This flowfield, however, reacts on thrust perturbations without time lag (see also reference 14). In reality, the time lag will lie between both extremes. By this means both curves correspond only partially with experimental data.

In comparison with the bearingless main rotor, the modal lead-lag damping of the tested bearingless MBB tail rotor lies about 0,5% crit.higher for zero thrust condition (see Figure 5.2).

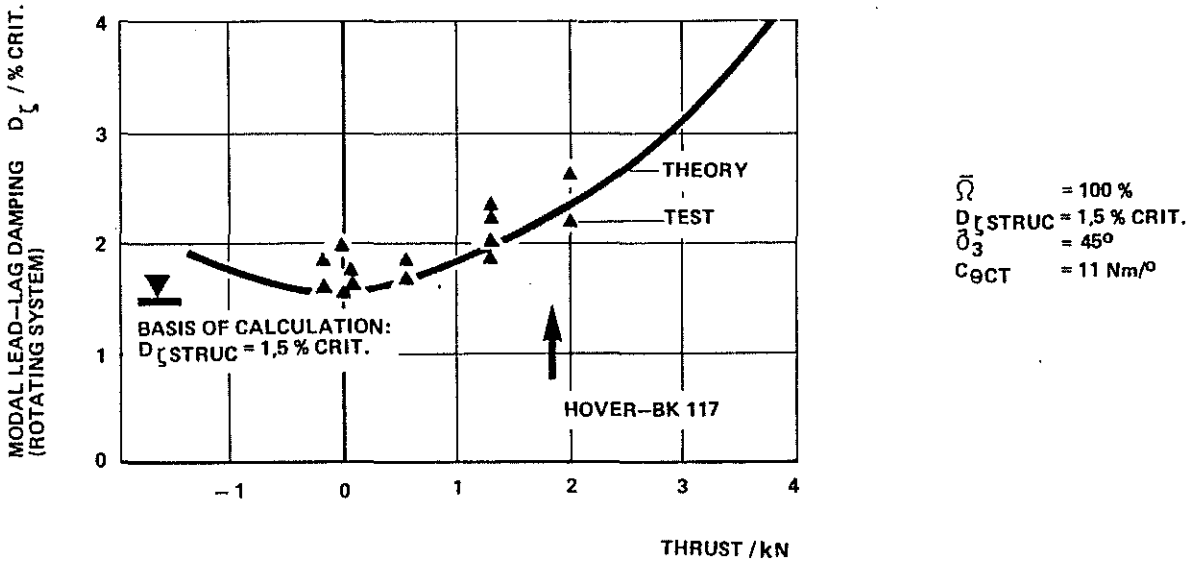

Figure 5.2 Lead-lag damping of bearingless tail rotor (theoretical and test stand results)

This is mainly provided by a higher inherent damping of the flexbeam ($D_{\zeta STRUC} \approx 1,5\%$ crit.), being equipped also with an integrated viscoelastic damper. Other important system data are:

- control stiffness	$C_{\theta CT} = 11$ Nm/°
- blade-to-beam angle	$\beta_{BB} = 0$
- constructive pitch-flap-coupling	$\delta_3 = 45°$
- equivalent flap hinge offset (without equivalent flapping restraint)	$\bar{a}_\beta = 2,4\%$

Because of the comparable agreement between experimental and theoretical results for both inflow models (see Figure 5.1), for Figure 5.2 and the following figures a global inflow model has been utilized.

5.2 Ground Resonance Prediction

Ground resonance evaluations have been conducted for the BO105, equipped with an experimental version of the bearingless main rotor using system parameters, introduced in section 5.1. (see Figure 5.3).

At the coalescence point of rotor lead-lag regressing mode frequency $\Omega - \omega_\zeta$ with the body pitch mode ($\bar{\Omega} \approx 104\%$) a negative damping $D_{\Omega-\omega\zeta} \approx -0,5\%$ crit. is expected. This proximity of ground resonance rotor speed and standard rotor speed led to a constructive stiffening of the BO105 landing gear and by this means to an offset of about 8% rotor speed between rotor resonance and standard speed. At standard rotor speed, a fixed system damping value $D_{\Omega-\omega_\zeta} \approx 1,5\%$ is now expected.

Ground resonance predictions for the bearingless tail rotor have been presented in reference 16.

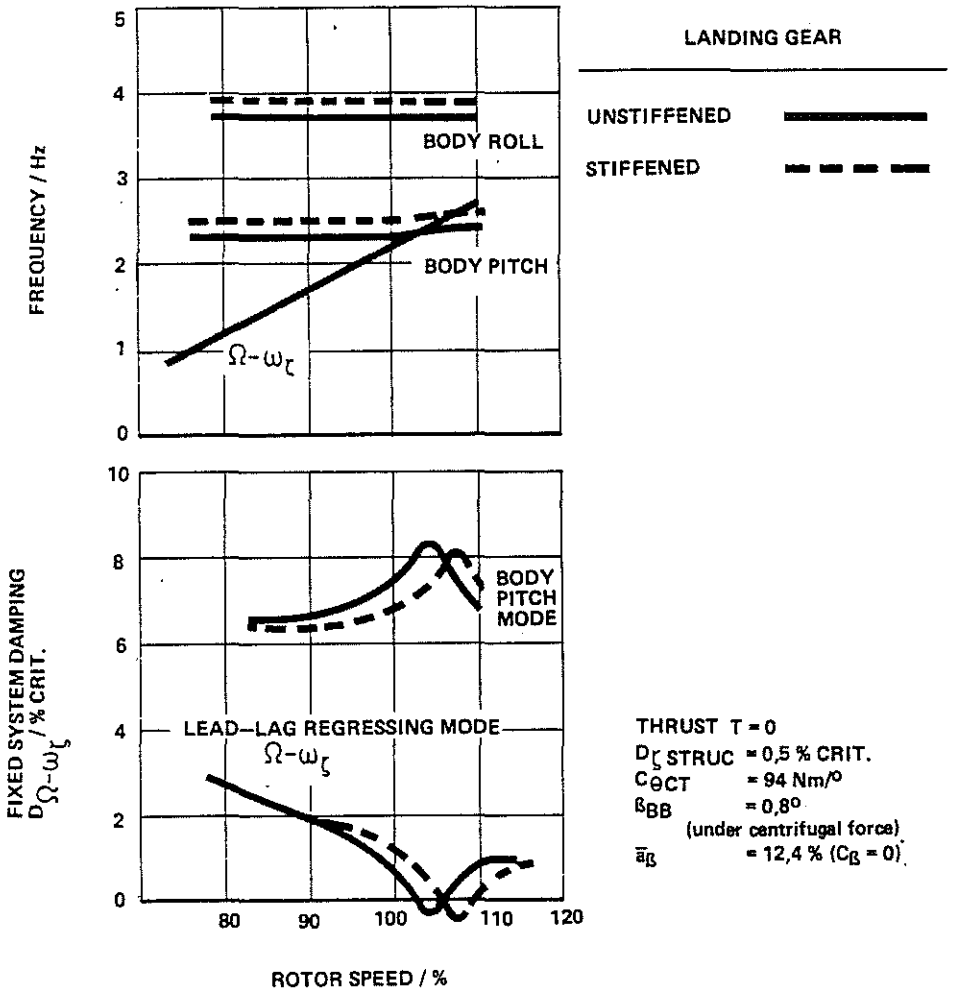

Figure 5.3 Ground resonance calculation of bearingless main rotor on BO105

6. Air Resonance Behaviour of Bearingless Main Rotor Systems

It is known that soft-inplane rotor systems are susceptible to air resonance (references 4,5,6). This phenomenon of rotor-body coupling can be influenced mainly by means of structural damping or bending-torsion coupling of the blade motion if a separation of the body and lead-lag regressing mode frequencies is not possible. In the following section, the most important parameters of the bearingless main rotor system affecting the air resonance behaviour by elastic bending coupling are discussed.

6.1 Aeroelastic Parameters

With the help of the simplified physical model, presented in chapter 4, the influence of the blade-to-beam angle on pitch-lag coupling (δ_1) was made apparent. Figure 6.1 verifies these reflections for a BO105 helicopter, equipped with a bearingless main rotor, showing lines of constant damping (% crit.) for the regressing rotor mode $\Omega-\omega_\zeta$, which derives from the more refined calculation method described in chapter 3. Having zero blade-to-beam angle and δ_1-coupling according to equ. 2, only the sum of structural and aerodynamic damping remains (about 2% crit.).

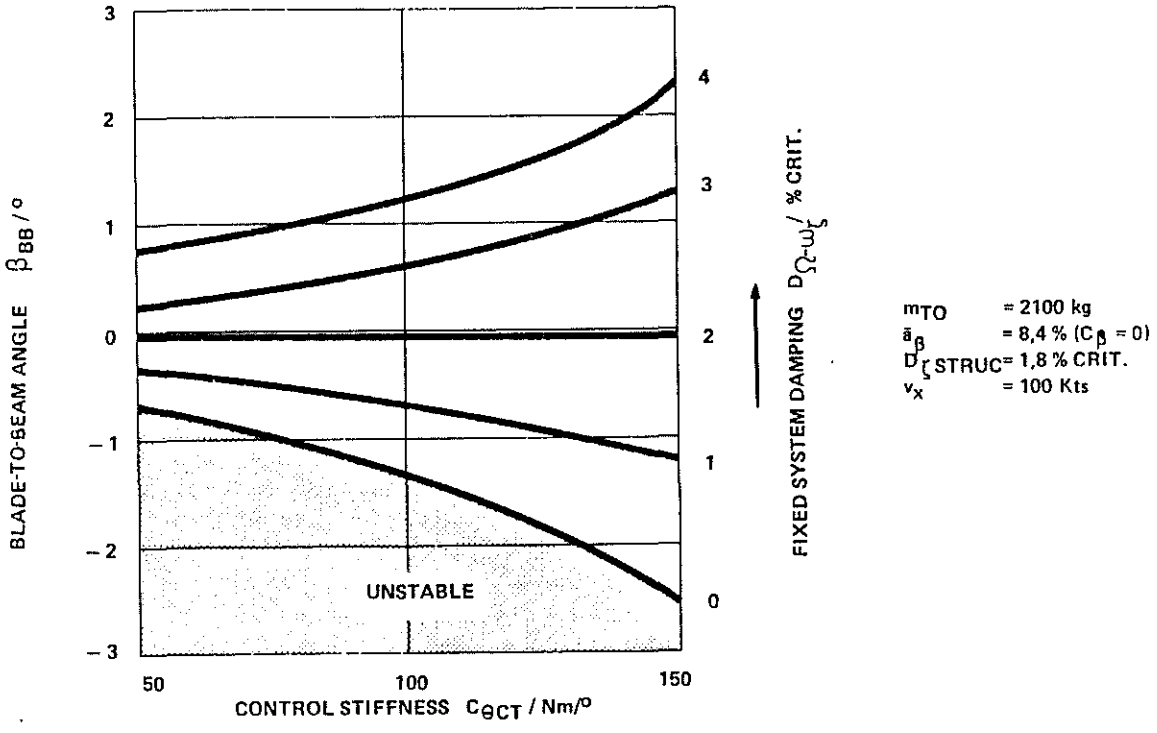

Figure 6.1 Influence of blade-to-beam angle and control stiffness of bearingless main rotor on fixed system damping

Figure 6.1 shows also that an aeromechanical instability may occur at negative blade-to-beam angles.

In Figure 6.2 the damping ratio of the Ω-ω_ζ mode is plotted against δ_1-coupling angle, showing an almost linear correlation in the range of the investigated parameter field.

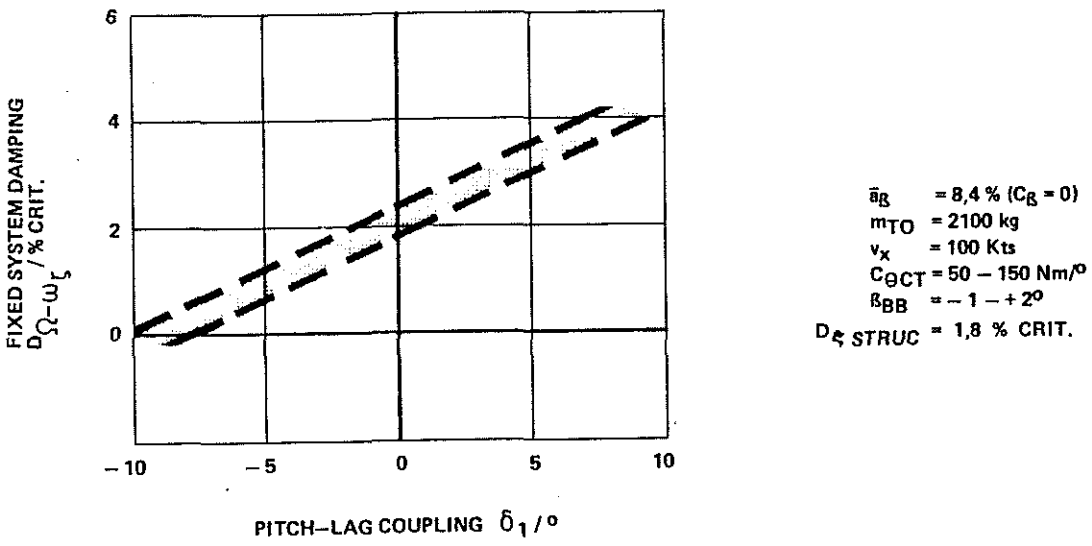

Figure 6.2 Fixed-system damping (regressive mode) $D_{\Omega-\omega_\zeta}$ versus pitch-lag coupling of bearingless main rotor

The scatter of the shadowed line is, on the one hand, an indication for the existence of higher harmonics of blade motion, owing to the unsymmetric flow condition at the rotor in forward flight. On the other hand, it stems from the non-uniformity of the δ_1 value during one rotor rotation, visible from the finite width of the torsion-lag ellipse in Figure 4.1 and 4.2.

Lower equivalent flap hinge offsets were also investigated during development of new bearingless rotor systems because of their easy applicability to this type of rotor system (reference 3). Generally, there is a trend to reduce the fundamental flap bending frequency of main rotor blades below 1.08 • Ω, corresponding to a virtual flapping hinge offset of less than 10% • R (reference 18).

Conflicting tendencies, dependent on flapwise bending stiffness, exist with regard to flight mechanics and handling qualities, concerning topics such as control characteristics, response cross-coupling, dynamic stability, and vibration sensitivity. Optimization towards a favourable bending stiffness has to be a compromise with respect to the particular helicopter's operational role. Figure 6.3 depicts the influence of equivalent flap hinge offset on air resonance behaviour.

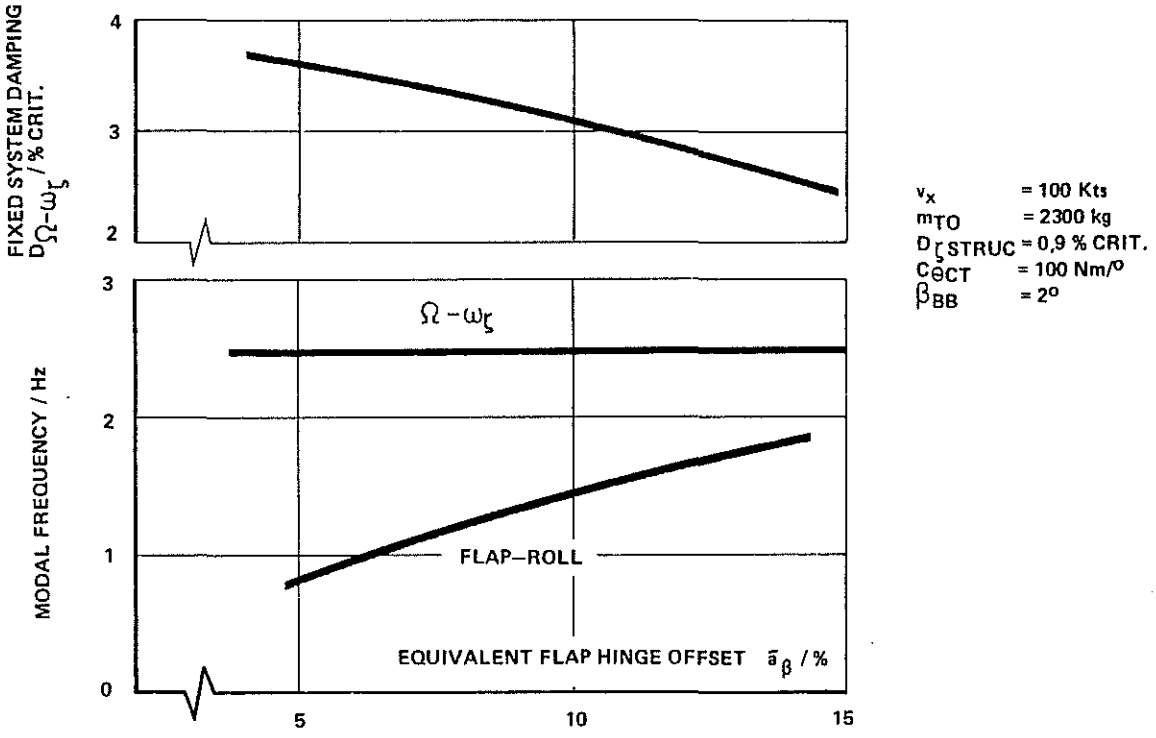

Figure 6.3 Air resonance characteristics of bearingless main rotor versus equivalent flap hinge offset

If the rotor system becomes less stiff, the frequency of the coupled rotor-body mode, which is in this case a flap-roll mode, decreases. On the other hand, the frequency of the $\Omega-\omega_\zeta$ mode is independent of flapwise bending stiffness and therefore the frequency difference of both modes increases, producing a higher damping ratio of $\Omega-\omega_\zeta$ mode, inversely proportional to the equivalent flap hinge offset.

The influence of kinematic δ_3-coupling (see Figure 6.4) is similar to the flapwise bending stiffness.

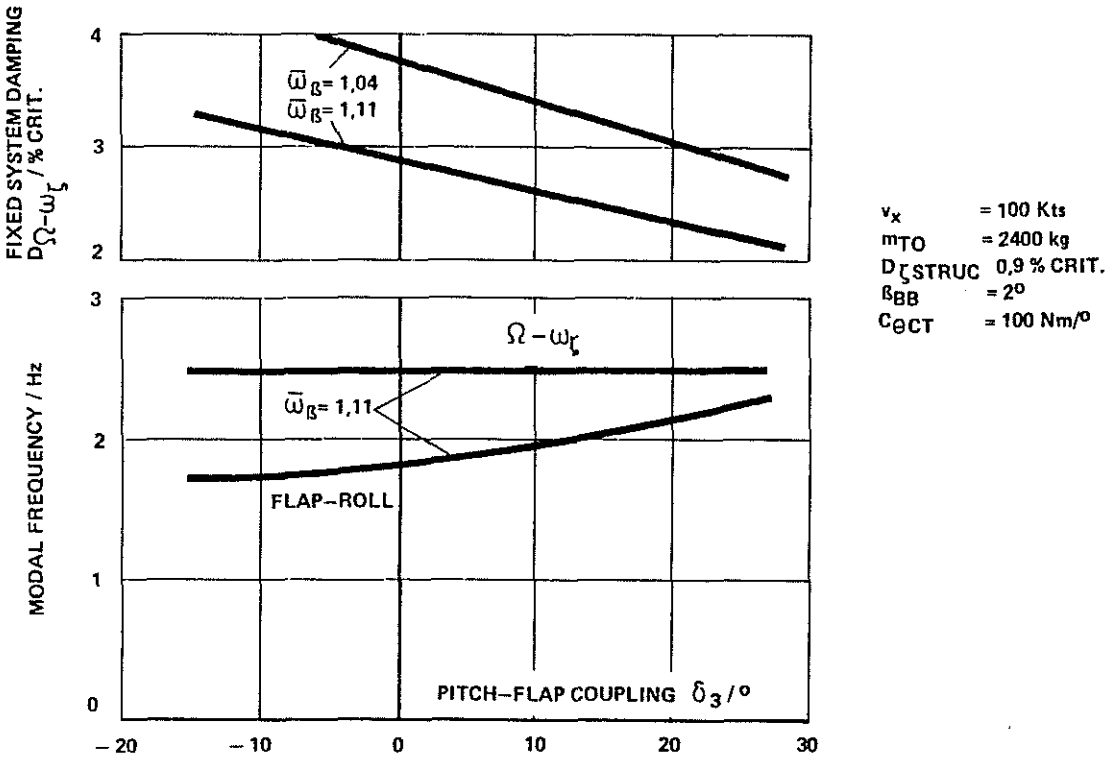

Figure 6.4 Air resonance characteristics of bearingless main rotor versus pitch-flap coupling

Positive δ_3 additionally raises the flapping natural frequency as well as increasing flap hinge offset. The reason is that with positive δ_3, the blade pitch is reduced as the blade flaps up and the downward aerodynamic flapping moment acts as a restoring spring, additional to the centrifugal force moment.

6.2 Prediction of Air Resonance Stability of Existing Rotor Projects

6.2.1 Stability of Bearingless Main Rotor, Experimental Version

Evaluations of air resonance stability of the bearingless main rotor (experimental version) on BO105 have been conducted for different flight velocities. Important system parameters and results are shown in Figure 6.5. For comparison, theoretical and experimental results of the BO105 hingeless system are noted (reference 15).

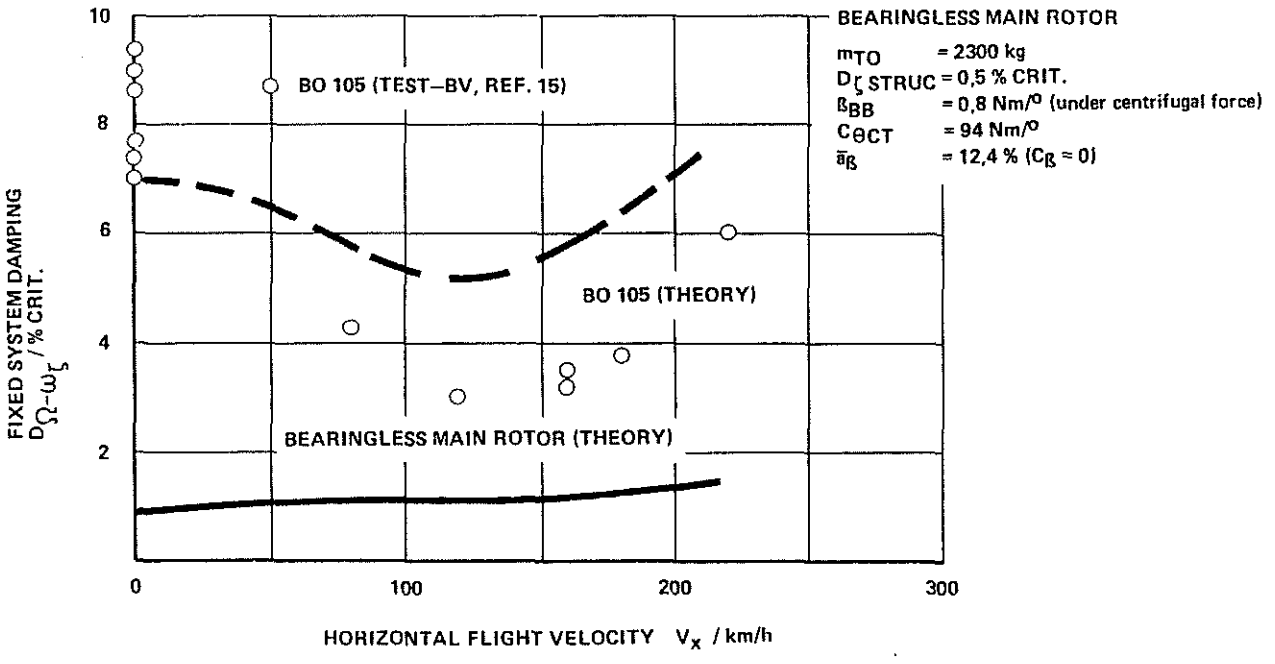

Figure 6.5 Air resonance stability of bearingless main rotor in forward flight (test helicopter BO 105)

The noticeably lower damping level of the experimental bearingless main rotor may be caused in this case by:

- a greater proximity of lead-lag regressing mode frequency and body roll mode frequency, owing to the higher natural lead-lag frequency of the bearingless main rotor,
- a lower inherent damping (see chapter 5.1 and reference 7)

As in the case of the whirl tower tests (chapter 5.1), centrifugal force reduces the built-in blade-to-beam angle to a certain extent, limitting by this means potential beneficial effects of δ_1-coupling.

As a consequence, an improvement of the damping situation is in hand for the prototype of the bearingless main rotor (Figure 1.1), under development at MBB.

6.2.2 Stability of Bearingless Tailrotor, Experimental Version

For soft-inplane tail rotors in air resonance conditions particularly rotor speed variations may become critical as for example in autorotation. Here the problem of coalescence between the rotor lead-lag regressing mode and a body mode frequency, normally far away from each other, may arise.

Figure 6.6 summarizes important system parameters and evaluation results of the bearingless tail rotor in its experimental version on a BK117-Helicopter.

Resonance occurs at $\bar{\Omega} \approx 94\%$ between the lead-lag regressing mode and the tail boom pitch mode which derives no benefit from the damping effects of the rotor disc as in the case of the yaw mode. Nevertheless there remains a damping level of about 2% crit. at the resonance point.

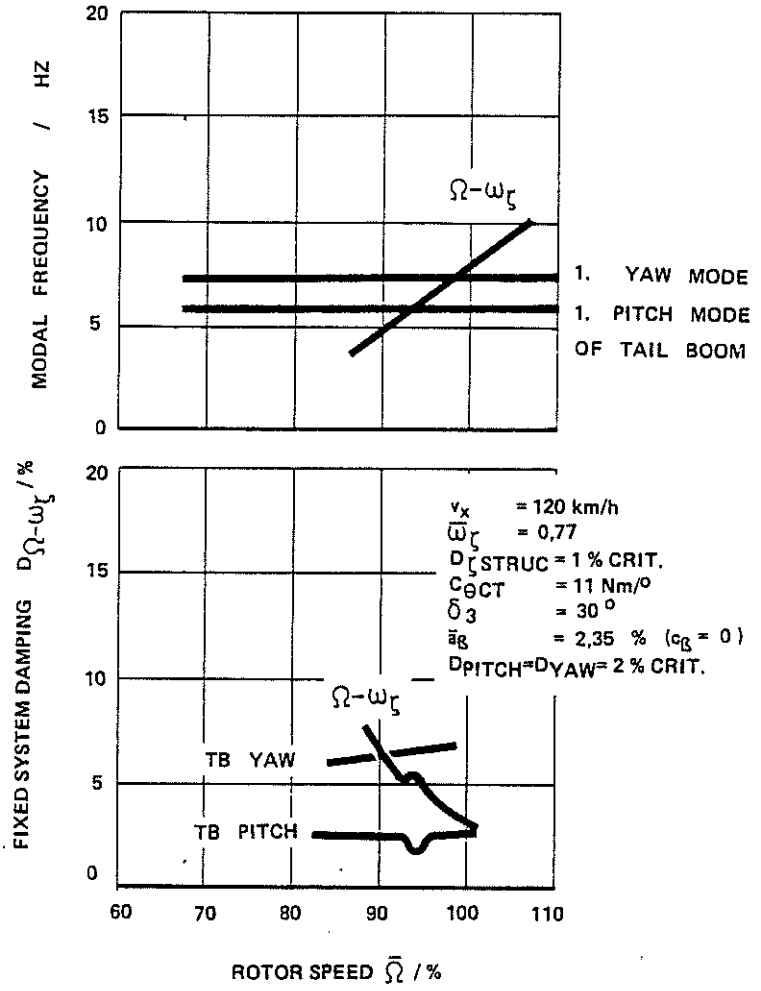

Figure 6.6 Air resonance stability of bearingless tail rotor on BK117 during autorotation (theoretical results).

6.3 Influence of Inherent Damping Models

Calculated system damping of the lead-lag rotor regressing mode at air resonance is strongly dependent on the inherent lead-lag damping model. Theoretical system damping results in this paper are commonly based on constant inherent damping values. However, depending on the actual rotor system, an influence of the lead-lag amplitude on inherent damping may occur. Figure 6.7 shows a comparison of fixed system damping ($D_{\Omega-\omega_\zeta}$) for:

- test results (reference 15),
- theoretical results with constant inherent damping, and
- theoretical results based on two non-linear inherent damping models.

The non-linear damping models take into account the measured dependency of inherent lead-lag damping from the alternating lead-lag moment at the blade root.

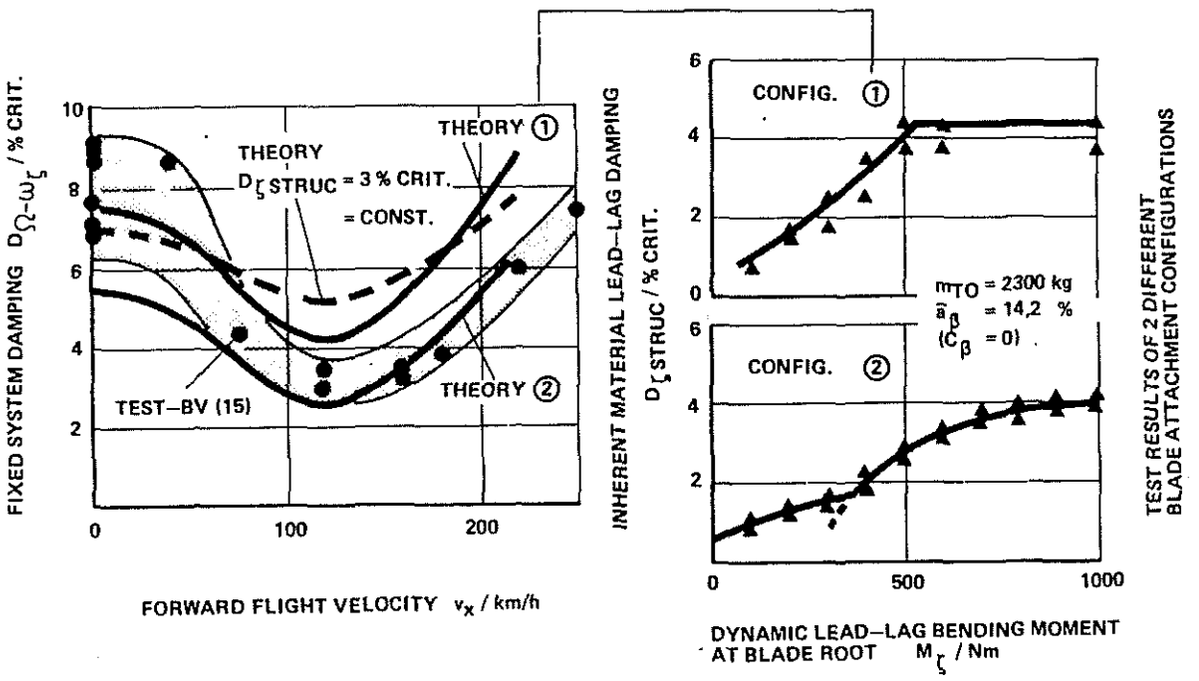

Figure 6.7 Influence of inherent damping modelling on air resonance evaluation (BO105 hingeless rotor system)

Apparently, the latter model shows the best coincidence with experimental damping values.

7. Conclusions

Bearingless rotor systems are particularly qualified for the use of elastic coupling effects. Here, mainly the blade-to-beam angle and the control stiffness are at the designer's disposal to provide pitch-lag coupling. This coupling can be utilized to increase the lead-lag damping in the rotating and in the fixed system for ground and air resonance conditions. However, attention is to pay to centrifugal force effects on the blade-to-beam angle.

Other parameters influencing the damping of the regressing mode of the lead-lag frequency are:

- helicopter body modes coupling with the regressing mode,
- pitch-flap coupling,
- flapping stiffness, and
- inherent material damping.

Not all parameters are in this case compatible or at the designer's disposal, so that compromises must be found.

8. References

1) H.B. Huber: Effect of Torsion-Flap-Lag Coupling on Hingeless Rotor Stability.
29th Annual National Forum of the American Helicopter Society, Washington D.C. 1973

2) Seth Dawson: An Experimental Investigation of a Bearingless Model Rotor in Hover.
Aeromechanic Laboratory, U.S. Army Research and Technology Laboratories, Moffet Field, California 94035

3) F.I. Mc Hugh, I.A. Staley, M.W. Sheffler: Dynamic Stability of Low Effective Flap Hinge Bearingless Main Rotor Concepts.
AHS Mideast Region, National Specialists' Meeting.
Rotor System Design, Philadelphia, Oct. 1980

4) Dewey H. Hodges: An Aeromechanical Stability Analysis for Bearingless Rotor Helicopters.
34th Annual National Forum of the American Helicopter Society, Washington D.C., May 1978, Preprint No. 78-21.

5) Robert A. Ormiston: Aeromechanical Stability of Soft Inplane Hingeless Rotor Helicopters.
Third European Rotorcraft and Powered Lift Aircraft Forum, Aix-en-Provence, France, Paper No. 25, September 7-9, 1977

6) W. Miao, H.B. Huber: Rotor Aeroelasticity Coupled with Helicopter Body Motion.
NASA SP-352, February 1974, PP. 137-146

7) James A. Staley, H.I. Mac Donald: Full Scale Ground and Air Resonance Testing of the Army-Boeing Vertol Bearingless Main Rotor.
35th Annual National Forum of the American Helicopter Society Washington D.C., May 1979, 79-23.

8) Ronald R. Fenaughty, William L. Noehren: Composite Bearingless Tail Rotor for UTTAS.
Journal of the American Helicopter Society, 22 (3), July 1977, pp.19-26.

9) John Shaw, W.Thomas Edwards, The YUH 61A Tail Rotor: Development of a Stiff Inplane Bearingless Flex-Strap Design.
Journal of the American Helicopter Society, 23 (2), Apr. 1978 pp. 9-18

10) James A. Staley, Richard Gabel, H.I. MacDonald: Full Scale Ground and Air Resonance Testing of the Army-Boeing Vertol Bearingless Main Rotor.
Paper No. 79-23, Proceedings of the 35th Annual National Forum of the American Helicopter Society, May 1979.

11) D. Banerjee, M. Ploudre: The YAH-64A Composite Flex-Beam Tail Rotor.
Paper No. I-3, Proceedings of the American Helicopter Society Mideast Region National Specialists' Meeting, Oct. 1980

12) H. Strehlow, B. Enenkl: Aeroelastic Design Considerations in the Development of Helicopters.
56th AGARD Structures and Material Panel Meeting, London, 10 - 15 April 1983

13) Troy M. Gaffey: The Effect of Positive Pitch-Flap Coupling (Negative δ_3) on Rotor Blade Motion Stability and Flapping.
Journal of the American Helicopter Society, April 1969.

14) D.A. Peters, G.H. Gaonkar: Theoretical Flap-Lag Damping with Various Dynamic Inflow Models.
35th Annual National Forum of the American Helicopter Society, Washington D.C. 1979.

15) P.G. Dixon: Design, Development, and Flight Demonstration of the Loads and Stability Characteristics of a Bearingless Main Rotor.
USAAVRADCOM-TR-80-D-3, June 1980.

16) H.Huber: Development of a Bearingless Helicopter Tail Rotor
Vertica, Vol. 5, 1981.

17) Robert A. Ormiston, Dewey A. Hodges: Linear Flap-Lag Dynamics of Hingeless Helicopter Rotor Blades in Hover.
Journal of the American Helicopter Society, Vol. 17, No.2, April 1972, pp. 2-4.

18) G. Seitz, G. Singer: Structural and Dynamic Tailoring of Hingeless/Bearingless Rotors.
9th European Rotorcraft Forum, Sept.83, Paper No. 60